Journal of Colloid and Interface Science 367 (2012) 40–48

Contents lists available at SciVerse ScienceDirect

Journal of Colloid and Interface Science

www.elsevier.com/locate/jcis

Using colloid lithography to fabricate silicon nanopillar arrays on silicon substrates

Jem-Kun Chen *, Jia-Qi Qui, Shih-Kang Fan, Shiao-Wei Kuo, Fu-Hsiang Ko, Chih-Wei Chu, Feng-Chih Chang

Department of Materials Science and Engineering, National Taiwan University of Science and Technology, 43, Sec. 4, Keelung Road, Taipei 106, Taiwan, ROC

ARTICLE INFO

Article history:
Received 15 February 2011
Accepted 17 October 2011
Available online 25 October 2011

Keywords:
Silicon nanopillar array
Very-large-scale integration
Colloidal lithography

ABSTRACT

In this study, we partially grafted geminal silanol groups in the protecting organic shells on the surfaces of gold nanoparticles (AuNPs) and then assembled the alkyl-AuNP-Si(OH)$_4$ particles onto the surfaces of silicon (Si) wafers. The density of assembled AuNPs on the Si surface was adjusted by varying the geminal silanol group content on the AuNP surface; at its optimal content, it approached the high assembly density (0.0254 particles/nm^2) of an AuNP assembled monolayer. Using reactive-ion etching (RIE) with the templates as masks, we transferred the patterned AuNP assemblies to form large-area, size-tunable, Si nanopillar arrays, the assembly density of which was controlled by the dimensions of the AuNPs. Using this colloidal lithography (CL) process, we could generate Si nanopillars having sub-10-nm diameters and high aspect ratios. The water contact angles of the high-aspect-ratio Si nanopillars approached 150°. We used another fabrication process, involving electron beam lithography and oxygen plasma treatment, to generate hydrophilic 200-nm-resolution line patterns on a Si surface to assemble the AuNPs into 200-nm-resolution dense lines for use as an etching mask. Subsequent CL provided a patterned Si nanopillar array having a feature size of 200 nm on the Si surface. Using this approach, it was possible to pattern sub-10-nm Si nanopillar arrays having densities as high as 0.0232 nm^{-2}.

1. Introduction

One of the most interesting research directions in the development of nanotechnology is the fabrication of ever-smaller nanostructures over large areas, ideally in a cost-effective way. Both fundamental research and industrial applications will benefit from the realization of simple approaches for the fabrication of nanostructures having feature sizes of less than 10 nm. The electronic structures of metal particles are influenced by their size when their dimensions are less than 5 nm. Recently, great effort has been expended to develop facile and reliable techniques for the fabrication of periodic nanostructures because of their potential impact on data storage [1,2], photonic crystals [3], and biological sensors [4–7]. Nanostructures constructed of nanoparticles (NPs) exhibit interesting electronic, optical, catalytic, and biological properties [8]. These materials include organic molecules, inorganic NPs, biological molecules, and small liquid droplets containing active components [9]. In particular, the fabrication of one-dimensional (1D) Au nanostructures from NPs has been investigated widely using a variety of techniques [10,11]. The resulting physical properties, which are those of neither the bulk metal nor the molecular components, strongly depend on the particle size, interparticle distance, nature of the protecting organic shell, and shape of the NPs [12,13]. The fabrication of ordered arrays of inorganic NPs remains a challenge because of the fundamental science associated with nanostructures and because of their technical applications [14]. To date, lithography has been the major workhorse method for generating NP arrays. The realization of these architectures has depended largely on the development of nanolithographic techniques, including microcontact printing [15], dip pen nanolithography [16], inkjet printing [17], and fountain pen-based printing [18]. In general, these methods rely on the transfer of molecules to chemically functionalized surfaces. Nonetheless, lithographic techniques are fairly expensive, complicated, and time-consuming, especially for the generation of large-area samples [19,20]. The throughput and controllability of NP deposition processes are poor. Therefore, many challenges remain in assembling and positioning NPs at desired locations to construct complex, functional structures.

Two-dimensional (2D) ordered micro/nanostructured arrays have recently received considerable attention because of their many potential applications. In the conventional techniques, colloidal lithography (CL) is an emerging technique for 2D nanopatterning [21]. The advantage that CL has over advanced lithographic techniques is that it allows the simple and rapid creation of large-area nanopatterns through the self-organization of colloids. A variety of unit patterns, ranging from dots to polygons, have been

* Corresponding author. Fax: +886 2 27376544.
E-mail address: jkchen@mail.ntust.edu.tw (J.-K. Chen).

0021-9797/$ - see front matter © 2011 Elsevier Inc. All rights reserved.
doi:10.1016/j.jcis.2011.10.044

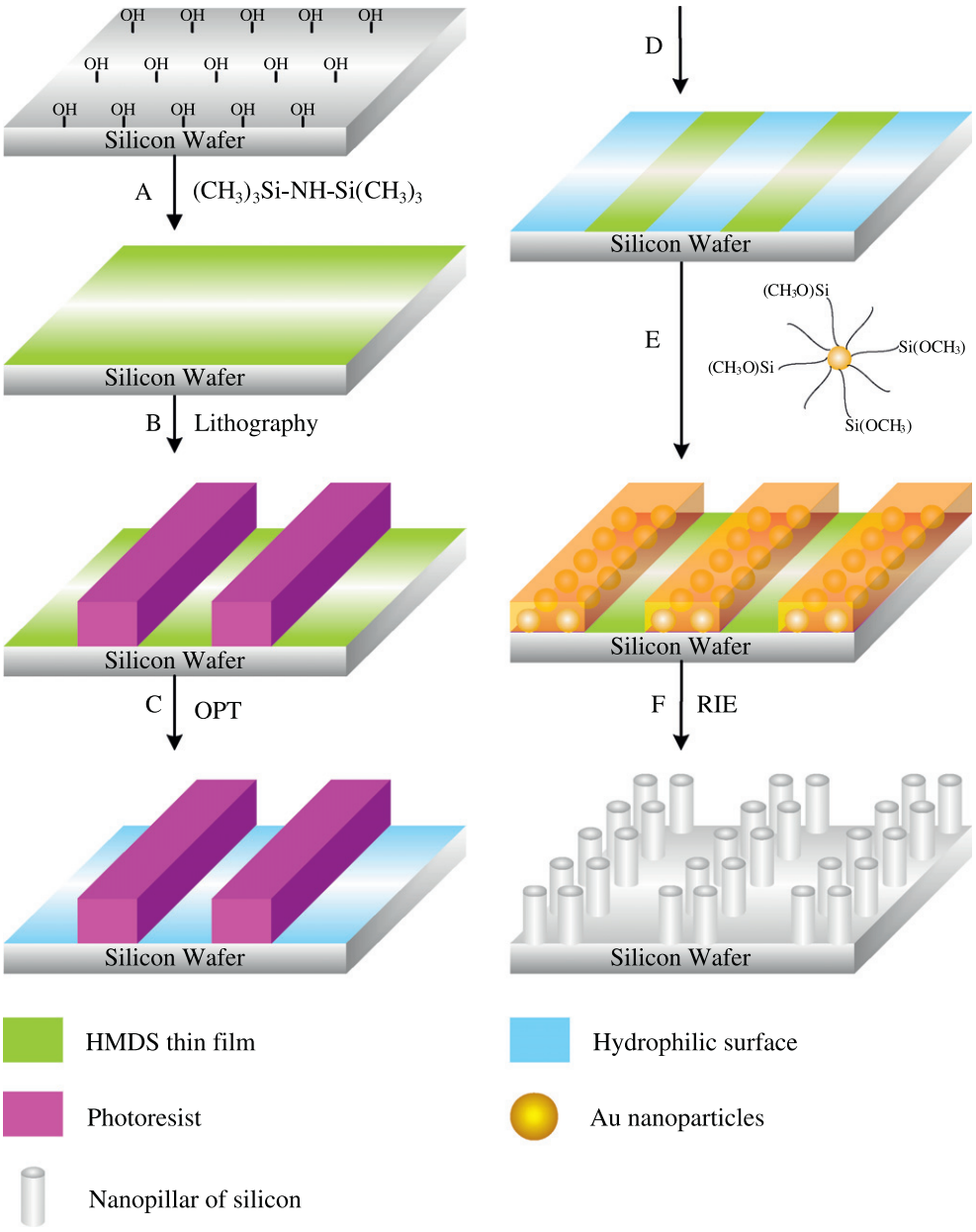

Fig. 1. Schematic representation of the direct patterning of a Si nanopillar array on a Si surface by using an AuNP monolayer as an etch mask in an RIE system. (A) The Si wafer is treated with HMDS. (B) E-beam lithography is used to pattern the photoresist with an array of trenches, with dimensions ranging from 200 nm to 10 μm after development. (C) The sample is subjected to OPT to form OH groups from the HMDS-treated surface. (D) The residual photoresist is removed from the surface to generate patterns of OH and HMDS-treated regions. (E) The Si substrate treated with HMDS and O_2 plasma is immersed in a colloid solution of alkyl-AuNP-$Si(OH)_4$ particles to immobilize AuNPs on the surface. (F) SF_6 and O_2 RIE (to open windows between the AuNPs) and CF_4 and Ar RIE (to create Si nanopillar arrays) are conducted sequentially.

fabricated through CL for their use in diverse applications [22]. Nevertheless, using CL to fabricate nanopillars and their 2D arrays remains a challenge because of the lack of controllability and the low aspect ratios of the resulting structures. Furthermore, most previous studies employing dry etching over a colloidal mask have produced dome-shaped structures rather than straight pillars. These unsolved issues arise mainly from (i) under-etching of the substrate around the contact point with the colloidal mask and (ii) simultaneous etching of both the mask and the substrate [23]. Recently, we developed a treatment process, similar to the one presented herein, for manipulating supported polymer brushes formed through bottom-up assembly [24]. We used this process to pattern functional groups over large areas with high throughout on the surfaces of silicon (Si) substrate. Here, we report a novel approach for fabricating Si nanopillar arrays by combining reactive ion etching (RIE) with gold nanoparticle (AuNP) assemblies as etch masks over Si substrates. Using this approach, we could control the densities of the Si nanopillar arrays simply by tuning the content of geminal silanol units in the protecting organic shells of the AuNPs.

2. Experimental section

2.1. Materials

Single-crystal Si wafers, Si(100), polished on one side (diameter: 6 in.) were supplied by Hitachi (Japan) and cut into 1 cm × 1 cm samples. The materials for the AuNP synthesis—hydrogen

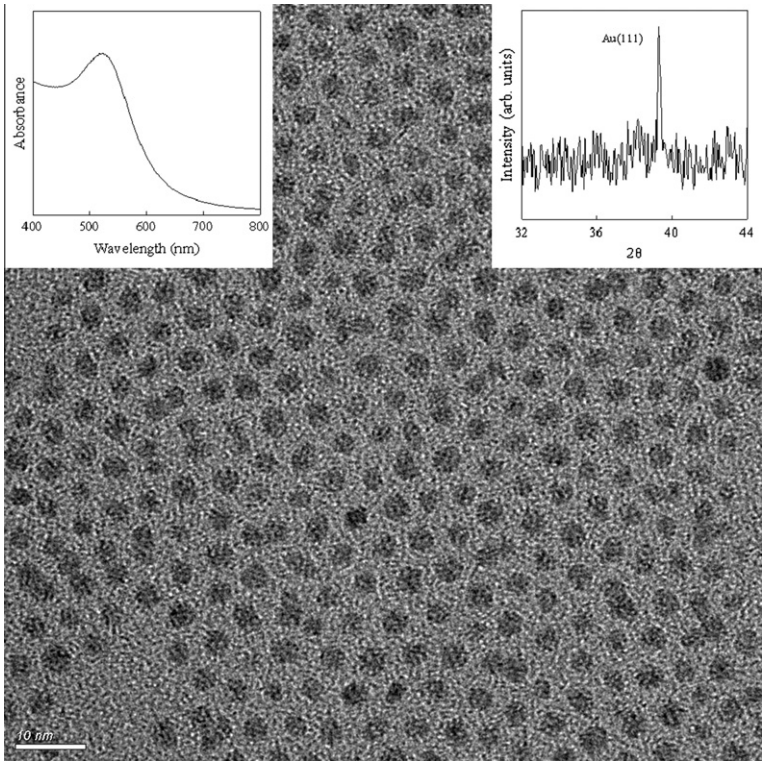

Fig. 2. TEM images, UV–Vis absorption spectrum (left corner), and the X-ray diffraction pattern (right corner) of the "free" alkyl-AuNP-Si(OH)$_4$ particles.

tetrachloroaurate(III) trihydrate ($HAuCl_4$), tetra-*n*-octylammonium bromide (TOAB; $C_{32}H_{38}BrN$), and sodium borohydride ($NaBH_4$)—were purchased from Acros Organics (American). The materials use to prepare the protecting organic shells—(3-mercaptopropyl)trimethoxysilane (MPTMOS) and dodecanethiol (DE)—were purified through vacuum distillation prior to use. The Si substrates were immersed in HF solution (50 wt.%) for 5 min at room temperature to remove the silicon oxide film. The HF-treated substrates were immersed in a mixture of HNO_3 and H_2O_2 (2:1, mol%) for 5 min and then rinsed with doubly distilled water at least three times to oxidize the Si. The Au clusters were fabricated with the simultaneous attachment of self-assembled thiol monolayers on the growing nuclei. To allow the surface reaction to occur during metal nucleation and growth, the particles were grown in a two-phase system [25]; $AuC1^{4-}$ ions were transferred from the aqueous solution to the toluene phase using TOAB as the phase-transfer reagent and reduced with aqueous $NaBH_4$ in the presence of mixtures of MPTMOS and DE (MPTMOS/DE = 10, 20, 30, 40, or 50 mol%) to form the protecting organic shells. Phase contrast images of the silanol- and alkyl-functioned AuNPs [alkyl-AuNP-Si(OH)$_4$] were obtained using a Philips Tecnai G2 F20 transmission electron microscope operated at an accelerating voltage of 200 kV (point resolution: 0.248 nm). The UV–Vis spectrum of the Au solution, obtained using a lambda 25 spectrophotometer (Perkin–Elmer), was similar to that of a gold hydrosol having an average particle diameter of 6 nm.

2.2. Fabrication of Si nanopillar arrays using AuNP assemblies as etch masks

Fig. 1 illustrates the strategy used to fabricate patterned Si nanopillar arrays using the very-large-scale integration (VLSI) process [26]. A: The Si wafer was treated with hexamethyldisilazane (HMDS) in a thermal evaporator (Track MK-8) at 90 °C for 30 s to transform the Si(OH)$_3$ groups on the surface of the wafer into an inert film of Si(CH$_3$)$_3$ groups. B: The photoresist was spun on the HMDS-treated Si wafer at a thickness of 780 nm; advanced lithography was then used to pattern the photoresist with an array of trenches having dimensions ranging from 200 nm to 10 μm after development [27]. C: The sample was subjected to oxygen plasma treatment (OPT) using a TCP 9400SE instrument (Lam Research) to form OH groups from the HMDS-treated surface; OPT caused the surface to become chemically modified (strongly hydrophilic or polar) only in the areas not covered by the photoresist; the introduction of these polar groups provided a more wettable surface for the preparation of a self-assembled monolayer of AuNPs. D: The remaining photoresist was removed from the HMDS-treated surface by rinsing with solvent, leaving behind the chemically nanopatterned surface. E: The Si substrate treated with HMDS and O_2 plasma was immersed in a toluene solution of alkyl-AuNP-Si(OH)$_4$ particles for 30 min at 25 °C to assemble the AuNPs on the surface; the alkyl-AuNP-Si(OH)$_4$ particles assembled selectively onto the bare regions of the Si surface after OPT, where they reacted with SiO and SiOO species; the Si substrates presenting assembled AuNPs were removed from the solution, washed with toluene for 15 min to remove any unreacted material, and dried under a stream of N_2. F: SF_6 and O_2 RIE (TCP 9400SE; Lam Research), for opening windows between the AuNPs, and CF_4 and Ar RIE, for the creation of the Si nanopillar arrays, were conducted sequentially. The appropriate RIE time was determined by examining the SEM image of the Si nanopillars. The feature sizes of the line patterns of the AuNP assemblies and of the Si nanopillar arrays were observed using high-resolution scanning electron microscopy (HR-SEM; JEOL JSM-6500F, Japan). The sheet resistances of the AuNPs at various assembly densities were measured using a four-point probe (Napson RT-70/RG-5, Japan). The modified surfaces for AuNP assembly were analyzed using ellipsometry (SOPRA SE-5, France) and X-ray photoelectron spectroscopy (XPS;

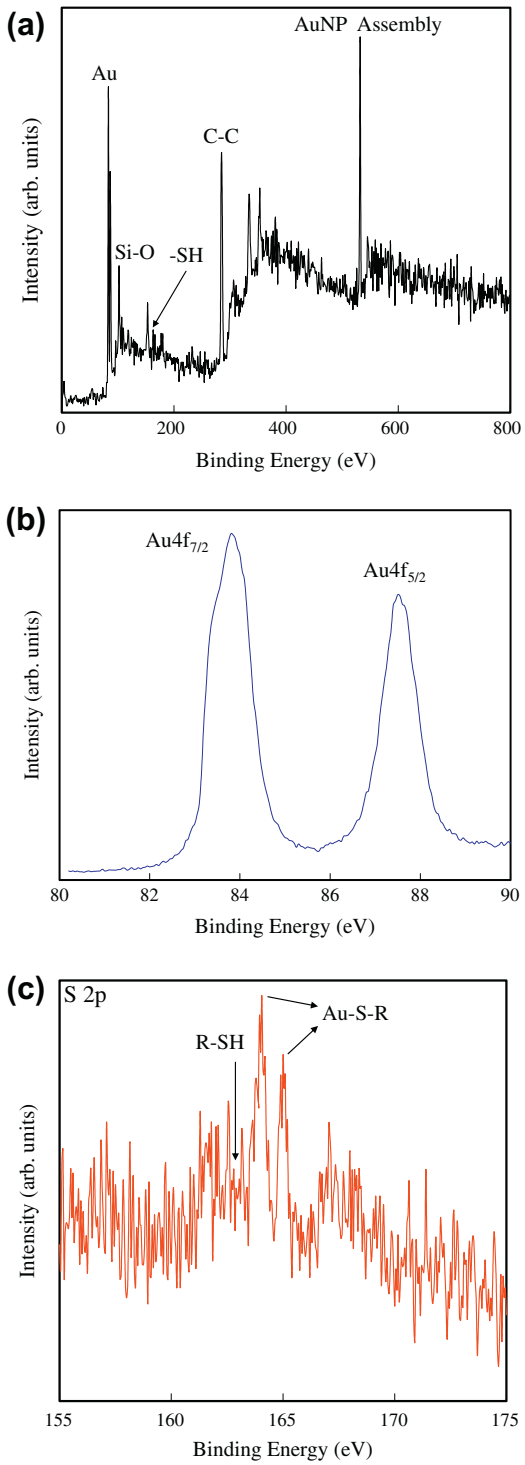

Fig. 3. (a) Wide-scan XPS spectra, (b) XPS Au 4f and (c) S 2p core-level spectra of the AuNP assemblies incorporating 30 mol% of MPTMOS in their protecting organic shells on the Si surfaces.

Scientific Theta Probe, UK). The XPS widescan spectra are at a take-off angles of $\alpha = 75^\circ$ for AuNP assemblies on silicon surface. Two Electrodes were fabricated to measure the resistivities of nanowires of the AuNP assemblies for five constructed layer with various resolutions by four-point probe (Napson RT-70/RG-5, Japan).

Table 1
Chemical composition of the AuNP assemblies incorporating 10, 20, 30, 40, and 50 mol% of MPTMOS in their protecting organic shells, determined from XPS core-level spectral area ratio.

MPTMOS content (%)	Chemical composition (%)			
	C	Si	Au	S
10	19.87	53.21	24.76	2.16
20	22.45	39.43	34.20	3.92
30	23.10	24.11	48.98	3.81
40	23.56	15.32	57.77	3.35
50	26.82	6.13	62.92	4.13

3. Results and discussion

3.1. Alkyl-AuNP-Si(OH)$_4$ immobilization for controllable assembly density

The high-resolution transmission electron microscopy (HR-TEM) image of the alkyl-AuNP-Si(OH)$_4$ particles in Fig. 2 reveals that they had diameters of 5–7 nm with a maximum particle size distribution at 6 nm. Examination of the specimens at higher resolution revealed a mixture of particle shapes, with a preponderance of cuboctahedral and icosahedral structures, similar to previous reports [28]. The X-ray diffraction (XRD) pattern in Fig. 2 (right corner) reveals a peak at 38°, corresponding to Au(1 1 1) [29]. In addition, the strong surface plasmon resonance band of the AuNPs (at ca. 525 nm) in the UV–Vis spectrum of the AuNPs in aqueous solution (Fig. 2, left corner) is indicative of crystalline Au cores [30]. The chemical compositions of the Si surfaces after assembling the alkyl-AuNP-Si(OH)$_4$ particles incorporating 30 mol% of MPTMOS was determined using X-ray photoelectron spectroscopy (XPS) as shown in Fig. 3 [31]. The wide-scan XPS spectra of the AuNP assemblies on the Si surfaces, recorded at takeoff angles (α) of 75°, revealed five obvious peaks at binding energies (BEs) of ca. 81–83 (attributable to AuNPs), 99–103 (attributable to Si–Si and Si–O species), 161–163 (attributable to thiolate species), 285 (attributable to C–C species), and 532 eV (Fig. 3a), suggesting that most of ions had been removed from the surface, which, therefore, approached an ion-free surface. The BEs of the doublet for Au 4f$_{7/2}$ (83.8 eV) and Au 4f$_{5/2}$ (87.5 eV) are characteristic of Au^0. The absence of a band at 83.5 eV, as found for Au^1 in gold thiol complexes, indicates that the Au atoms in the clusters were present largely in the form of Au^0. The gradual strengthening of the signals for Au 4f$_{7/2}$ (82.8 eV) and Au 4f$_{5/2}$ (86.5 eV) confirmed that the Si surface was ideally Au-terminated [32]. Treatment of the AuNPs with mixtures of MPTMOS and DE formed protecting organic shells presenting silanol- and alkyl-terminated surfaces (Fig. 3b). The S 2p peak appeared in the spectrum because of the partial content of thiol-capped AuNPs; it could be resolved into three components having BEs of 162, 164, and 165 eV, which we assign to unbound thiols (R–SH), and thiolates (Au–S–R) with S 2p$_{1/2}$ and S 2p$_{3/2}$ components, respectively (Fig. 3c) [33]. Consequently, the gold–thiol bond does not appear to have the character of a gold sulfide. We used the XPS data to perform elemental analyses of the AuNPs incorporating various MPTMOS contents. The chemical composition of S of the AuNPs increased linearly upon increasing the MPTMOS content. These results clearly suggested that the AuNPs are effectively capped with the silanol groups to immobilize the AuNP through covalent bond on the surface. We have summarized chemical compositions of the AuNP assemblies incorporating 10, 20, 30, 40, and 50 mol% of MPTMOS in their protecting organic shells in Table 1.

Fig. 4 displays SEM images (top views) of alkyl-AuNP-Si(OH)$_4$ particles, incorporating 10–50 mol% of MPTMOS, assembled on

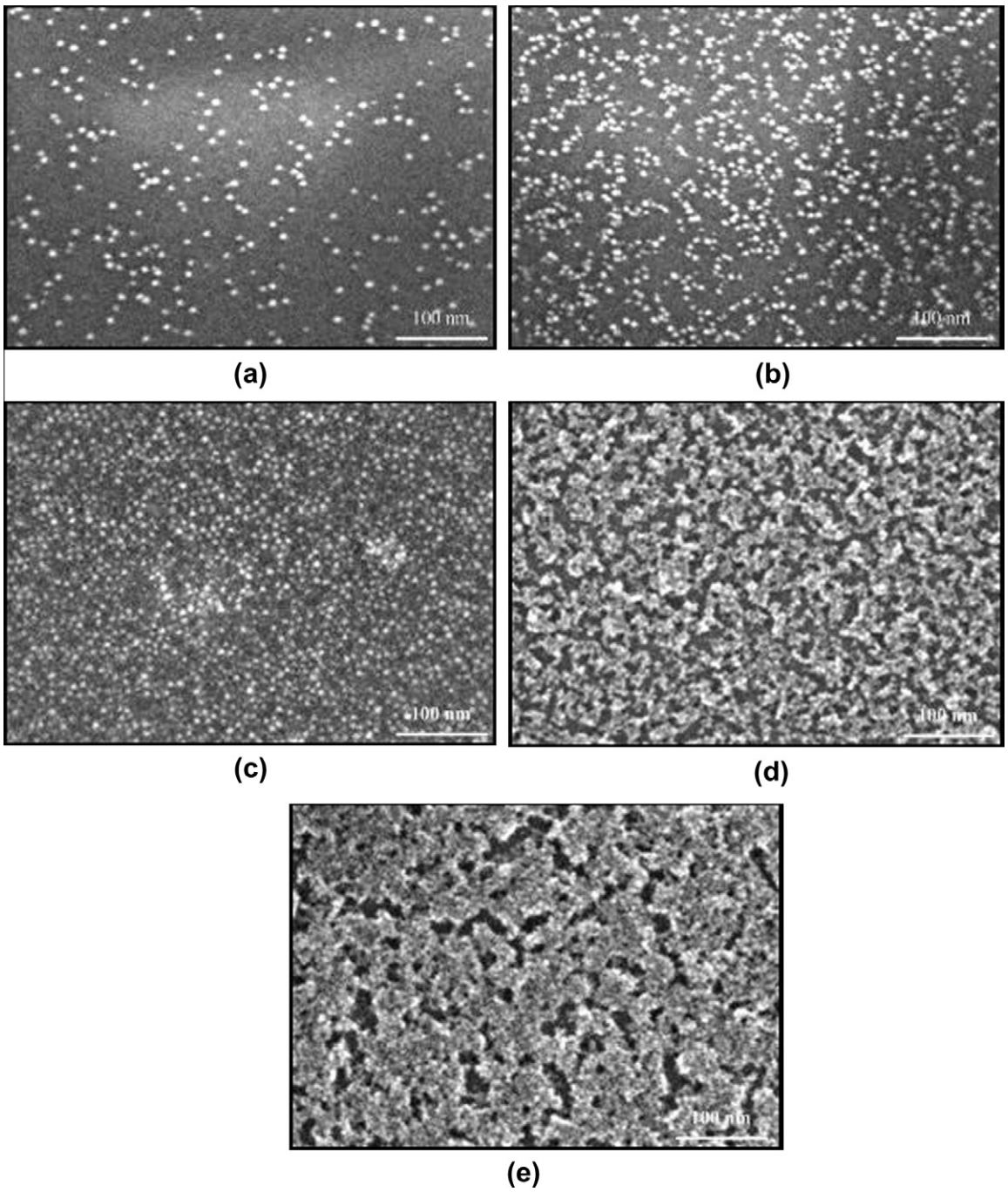

Fig. 4. Top-view SEM images of alkyl-AuNP-Si(OH)$_4$ particles incorporating: (a) 10, (b) 20, (c) 30, (d) 40, and (e) 50 mol% of MPTMOS self-assembled on their surfaces.

non-patterned Si surfaces. The alkyl-AuNP-Si(OH)$_4$ particles reacted with OH groups on the Si surfaces, thereby becoming immobilized. The alkyl-AuNP-Si(OH)$_4$ particles incorporating 10 mol% MPTMOS were immobilized on the surface with little interparticle cross-linking; the interparticle distance among the AuNPs was irregular, at 10–60 nm (Fig. 4a). The degree of interparticle cross-linking increased gradually, with decreasing interparticle separation, upon increasing the MPTMOS content in the alkyl-AuNP-Si(OH)$_4$ particles, leading ultimately to the assembly of an AuNP monolayer on the surface (Fig. 4b). A higher-density, regular AuNP monolayer was assembled from the alkyl-AuNP-Si(OH)$_4$ particles incorporating 30 mol% of MPTMOS on the surface, minimizing the average interparticle distance between the AuNPs (Fig. 4c). The TEM image in Fig. 2 was obtained from dispersed alkyl-AuNP-Si(OH)$_4$ in colloid solution. Because AuNP dispersed stably in the colloid solution, the well-ordered AuNP image could be observed by TEM. When we spin-coated the colloid solution including alkyl-AuNP-Si(OH)$_4$ on the surface for fabrication of nanopillar, the disordered AuNP monolayer on the surface were obtained (Fig. 4a–c). The immobilized AuNP monolayers were generated through a combination of interparticle cross-linking and interfacial cross-linking between the particles and the Si surfaces. Increasing the MPTMOS content above 40% led to the alkyl-AuNP-Si(OH)$_4$ particles assembling in the form of multi-layers on

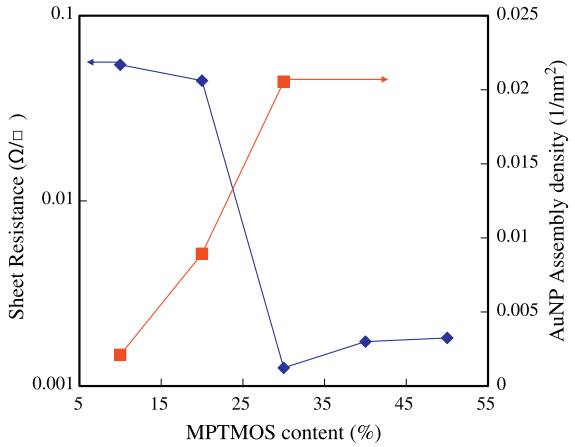

Fig. 5. Sheet resistance and assembly density of AuNPs on the surfaces plotted with respect to the MPTMOS content in the protecting organic shells of the alkyl-AuNP-$Si(OH)_4$ particles.

the surfaces (Fig. 4d and e) as a result of high densities of interparticle cross-links. Thus, appropriate control over the content of geminal silanol groups presented from the alkyl-AuNP-$Si(OH)_4$ particles can induce the AuNPs to self-assemble into the form of an immobilized 2D high-density monolayer on the Si surface. Fig. 5 displays the average assembly densities of the AuNP on the Si surfaces, as calculated from the SEM images. An approximately linear increase in the assembly density of AuNPs on the Si surface occurred upon increasing the MPTMOS content up to 30 mol%. Thus, the assembly density of the AuNPs on the Si surface could be adjusted merely by changing the MPTMOS content in the protecting organic shells of the AuNPs. Fig. 5 also displays the sheet resistances for the various densities of the AuNP assemblies on the Si surfaces, as obtained through four-point probe measurement; here, we employ a logarithmic scale for the sheet resistance to diminish the effects of environmental factors (e.g., noise, humidity, static electricity in the air) that might affect the results. The lowest sheet resistance on the surface occurred for the AuNP monolayer self-assembled from alkyl-AuNP-$Si(OH)_4$ particles incorporating 30 mol% of MPTMOS. The results are consistent with the fact that NPs having diameters in the range 1–10 nm would display electronic structures, reflecting the electronic band structures of the NPs, owing to quantum mechanical rules [34,35]. In addition, the SiO_2 thin films generated from the MPTMOS units on the AuNP surfaces blocked electron drafting and tunneling among the assembled AuNPs, resulting in increased sheet resistance for the multi-layer AuNP assemblies.

3.2. Silicon nanopillar arrays prepared using AuNPs as etch masks

To fabricate Si nanopillar arrays, we placed the substrates presenting monolayer AuNP assemblies in a reactive ion etcher. After the etcher had been evacuated to less than 1.8×10^{-3} Pa, the substrates were cleaned with O_2 plasma (50 mtorr, 100 W) for 30 s, and then a mixture of CF_4 (10 sccm) and Ar (10 sccm) at a total pressure of 100 mtorr was applied for 1–5 min. Tilted-view (15° oblique angle) SEM images (Fig. 6) reveal the surfaces obtained after CF_4 and Ar RIE processing for 5 min of the assembled AuNP monolayers (0.0025, 0.0089, and 0.0254 particles/nm^2) and multi-layers used as masks. We obtained high-aspect-ratio, sub-10-nm Si nanopillars with various densities on the surfaces (cf. high magnification images in Fig. 6a–c). The average diameter of the features at the tips of the Si nanopillars was ca. 6 nm, corresponding to the average diameter of the AuNPs. The average diameters at the bases of the Si nanopillars generated from the assembled AuNPs at densities of 0.0021 and 0.0089 particles/nm^2 were ca. 31 nm; therefore, they displayed obvious cone-like structures (Fig. 6a and b) [36], consistent with those reported previously, but with higher aspect ratios [37]. We obtained Si nanopillars with needle-like structures when using the surface of the assembled AuNPs at an assembly density of 0.0254 particles/nm^2 as the etch mask (Fig. 6c) [38]. The observation suggests that the cone-like structures of the Si nanopillars transformed gradually into needle-like structures upon increasing the assembly density of the AuNPs in the etch masks for the RIE process. The densities of the Si nanopillar arrays prepared from the surfaces presenting the assembled AuNPs at densities of 0.0025, 0.0089, and 0.0254 particles/nm^2 were ca. 0.0025, 0.0083, and 0.0232 nm^{-2}, respectively; that is, they corresponded approximately to the densities of the etch masks on the surface. The heights of the nanopillars generated from the assembled AuNPs at densities of 0.0021, 0.0089, and 0.0254 particles/nm^2 used as masks for RIE processing for 5 min were 68.7, 78.1, and 84.5 nm, respectively (cf. Fig. 4a–c). Therefore, this method allows Si nanopillar arrays having very high aspect ratios to be produced over large domains. Although the size of a typical perfect domain was ca. 400–800 μm^2, the entire surface of the substrate was covered with domains of nanopillar arrays. The overall defect concentration was less than 10% of the overall area. Fig. 6d displays the Si nanopillars obtained after RIE processing using multi-layer Au assemblies as etch masks. The average diameter of the features at the tips of the Si nanopillars approached ca. 28 nm—much larger that the AuNPs, presumably because cross-linked AuNP assemblies acted as etch masks in this RIE process. The multi-layer Au assembly on the surface resists RIE, thereby decreasing the height of the Si nanopillars to ca. 44 nm. Further increasing the degree of AuNP cross-linking in the etch mask caused the CF_4 and Ar RIE gasses to pass through the intervals among the cross-linked AuNP assemblies to etch the surface anisotropically and form a rough surface lacking nanopillar structures (Fig. 6e). Thus, an appropriate assembly density of AuNPs provides high contrast to poly-Si for CF_4/Ar RIE of the surface, resulting in highly selective etching to fabricate Si nanopillars on the surface. The nanopillars could not be fabricated completely by using high density AuNP assembly as etching mask, because AuNP assembly covered all over the surface. Fig. 7 displays the heights of the Si nanopillars formed after RIE processing using the AuNP assemblies (0.0021, 0.0089, and 0.0254 particles/nm^2) as etching masks, plotted with respect to the etching time. The results suggest that the etching rate of the CF_4/Ar RIE for poly-Si increased upon increasing the assembly density of AuNPs in the etch mask on the surface.

Because of their fascinating self-cleaning properties (nanostructured) superhydrophobic surfaces have recently become the focus of considerable scientific and technological interest [36]. Therefore, we investigated the hydrophobicities of our Si nanopillar arrays. Fig. 8a and b displays top-view SEM images of the Si nanopillar arrays having densities of 0.0083 and 0.0232 nm^{-2}, respectively, as well as photographic images of water droplets on these surfaces; Fig. 6b and c provide the cross-sectional morphologies of these surfaces. The SEM images reveal that the average diameters of the nanopillars were ca. 6 nm, with small gaps between the Si nanopillars (<30 and <10 nm for the arrays having densities of 0.0083 and 0.0232 nm^{-2}, respectively). The water contact angles (WCAs) of the Si nanopillar surfaces featuring array densities of 0.0083 and 0.0232 nm^{-2} were 150 ± 5° and 145 ± 4°, respectively. Fig. 9 reveals that the WCAs of the surfaces presenting Si nanopillar arrays increased upon increasing the etching time, because of the increased aspect ratios of the Si nanopillars. With their lack of any obvious nanostructures, the Si surfaces that we had etched through the multi-layer AuNP assemblies as etch masks did not exhibit hydrophobic properties. Our results suggest that the surface

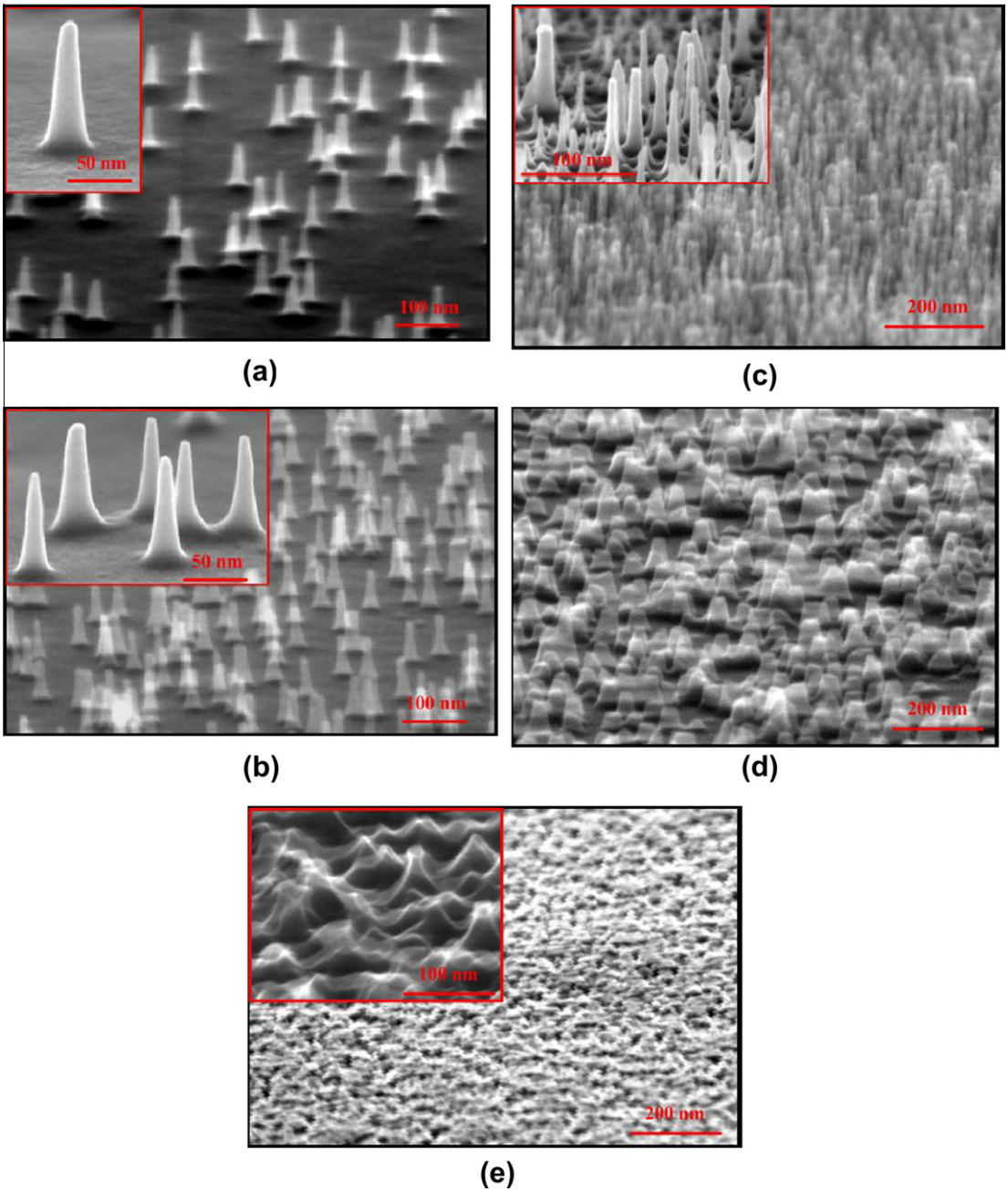

Fig. 6. Titled-view (15° oblique angle) SEM images of the surfaces obtained after RIE processing using AuNP assemblies, incorporating: (a) 10, (b) 20, (c) 30, (d) 40, and (e) 50 mol% of MPTMOS in their protecting organic shells, as etch masks to generate Si nanopillars on the surfaces. High-magnification images are provided in the left-hand corners of (a–c and e).

properties of the Si arrays featuring nanopillar densities of 0.0083 and 0.0232 nm^{-2} approach superhydrophobicity. In addition, we summarized dynamic and static contact angles measured on the nanopillars (Fig. 6) after RIE processing for 5 min using AuNP assemblies, incorporating (a) 10, (b) 20, (c) 30, (d) 40, and (e) 50 mol% of MPTMOS in their protecting organic shells, as etch masks to generate Si nanopillars on the surfaces in Table 2. Both the nanopillars, generated by RIE processing for 5 min using AuNP assemblies, incorporating 20, and 30 mol% of MPTMOS, as etch masks show a small contact angle hysteresis (<10°), which is much less than that of other nanopillar surfaces. The underlying reason is that the hairlike nanopillars present a discontinuous three-phase contact line with the water droplet, decreasing friction and lowering the energy barrier for the advancing and receding drop [39] When the flat surface comprised of the nanopillars was tilted to 3° relative to the horizontal, a 5 mg water droplet began rolling because of gravity. This suggests that the adhesion force between the water drop and the structured nanopillar surface is small.

Our final step in this study was the immobilization of alkyl-AuNP-$(SiOH)_4$ particles on OH-functionalized areas of patterned Si surfaces. The incorporation of reactive OH groups after OPT allowed their direct use in the assembly of AuNPs. The top-view SEM images in Fig. 10a confirm the success of the AuNP assembly on the patterned OH-functionalized Si surface into a spatially localized assembled AuNP monolayer when using the AuNP-$(SiOH)_4$ particles incorporating MPTMOS at a content of 30 mol%. We use

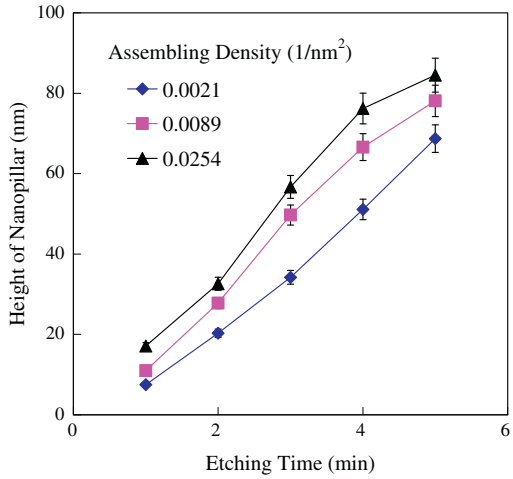

Fig. 7. Average height of the Si nanopillars plotted with respect to the etching time when using assembled AuNPs at densities of 0.021, 0.089, and 0.0254 particles/nm^2 as etch masks.

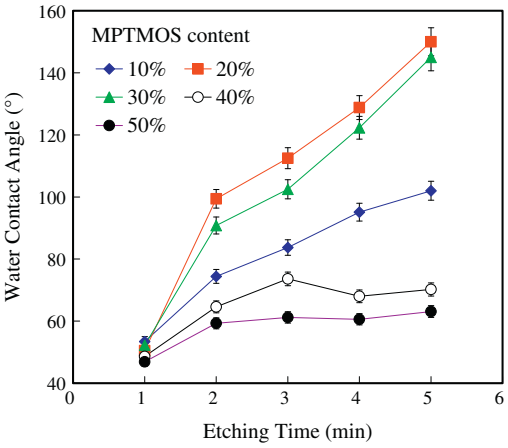

Fig. 9. WCAs of Si nanopillar surfaces plotted with respect to the etching time when using assembled AuNPs at densities of 0.0021, 0.0089, and 0.0254 particles/nm^2 as etch masks.

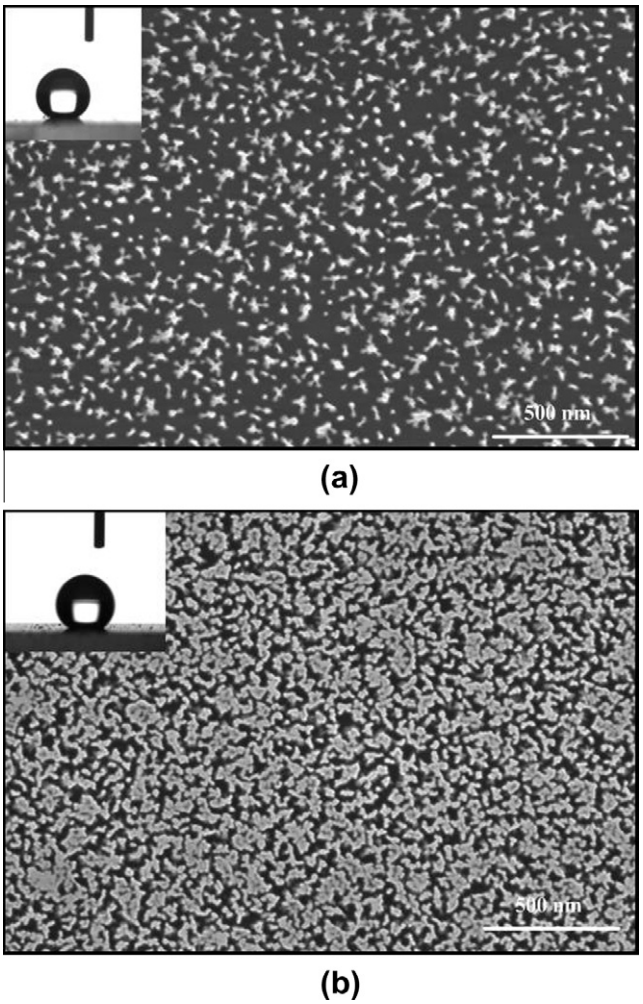

Fig. 8. Top-view SEM images of Si nanopillars generated by using assembled AuNPs at densities of 0.0089 and 0.0254 nm^{-2} as etch masks. A photographic image of a droplet is provided in the left-hand corner, with an illustration of the cross-sectional morphology.

Table 2
Dynamic and static contact angles measured on the nanopillars (Fig. 6) after RIE processing for 5 min using AuNP assemblies, incorporating: (a) 10, (b) 20, (c) 30, (d) 40, and (e) 50 mol% of MPTMOS in their protecting organic shells, as etch masks to generate Si nanopillars on the surfaces.

MPTMOS content (%)	Advancing contact angle (°)	Receding contact angle (°)	Contact angle hysteresis (°)	Max static contact angle (°)	Sliding angle[a] (°)
10	107 ± 3	92 ± 3	15	102 ± 3	6 ± 3
20	150 ± 5	141 ± 5	9	150 ± 5	2 ± 2
30	147 ± 5	139 ± 4	8	145 ± 4	3 ± 1
40	74 ± 4	52 ± 3	22	70 ± 4	11 ± 3
50	66 ± 3	38 ± 3	28	63 ± 3	17 ± 2

[a] Tilted angles at which the water droplet begins to roll are also listed.

lithography processes with positive photoresists to fabricate trenches (duty ratio = 1:1) with resolutions ranging from 200 nm to 10 μm. The AuNP-$(SiOH)_4$ particles assembled on the OH groups of the trenches to form a patterned assembled AuNP monolayer featuring a line resolution of 200 nm. After RIE processing, using the 200-nm-resolution line pattern of the assembled AuNP monolayer as an etch mask, we obtained line patterns of Si nanopillar arrays on the surface (duty ratio = 1:1) with a resolution of 200 nm (Fig. 10b). Although several AuNPs absorbed on the HMDS-treated surface to generate single Si nanopillars, most of the Si nanopillars were located on the trenches patterned through a combination of e-beam lithography and OPT. The nanopillars existed in the undesired area might affect the performance of the device. We are trying to surmount this problem by two processes. Transforming alkyl-AuNP-$Si(OH)_4$ on the surface directly by printing technology may reduce these nanoparticles in undesired area.

4. Conclusion

We have developed an approach for producing large-area, well-defined patterned Si nanopillar arrays having a feature size of less than 10 nm. Capping geminal silanol groups onto the surfaces of AuNPs allowed their assembly from the colloid solution onto Si surfaces; monolayers could be formed from the CL process by adjusting the silanol content of the AuNPs. This approach allows the direct manipulation of AuNPs on the Si surface. The AuNP assemblies on the Si surfaces exhibited significant variations in their electrical sheet resistances because of the effects of electronic

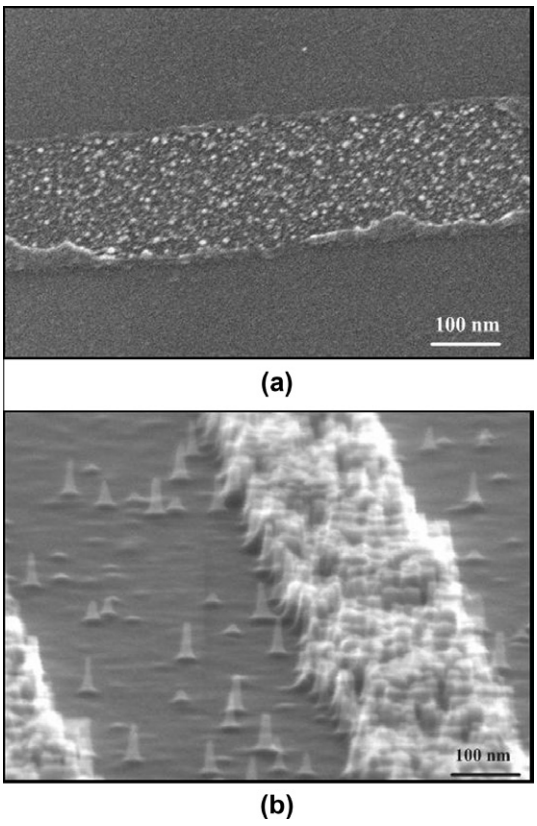

Fig. 10. (a) Top-view SEM image of AuNPs assembled in the 200-nm-resolution trench of a line pattern. (b) Titled-view (15° oblique angle) SEM image of Si nanopillars assembled as line patterns on the Si surface, generated by using the 200-nm-resolution line pattern of assembled AuNPs as an etch mask in the RIE process.

drafting and tunneling. Furthermore, we used the AuNP assemblies as etching masks against the RIE process to generate high-aspect-ratio Si nanopillar arrays on the Si surfaces. The densities of the Si nanopillars after RIE processing correlated approximately to the assembly density of AuNPs; the properties of the nanopillar structures approach superhydrophobicity. We also combined our developed method with VLSI processing to prepare Si nanopillar arrays in precisely controlled positions over large areas with high throughout. We suspect that nanopillar arrays generated using this approach might be useful for producing NPs via printing lithography methods (e.g., nanoimprinting lithography) and for the nanofabrication of electrodes and electronic and nanophotonic devices (e.g., photoluminescence sensors).

Acknowledgment

We thank the National Science Council of the Republic of China for supporting this research financially and the National Nano Device Laboratories for fabrication support.

References

[1] J.Y. Cheng, C.A. Ross, V.Z.H. Chan, E.L. Thomas, R.G.H. Lammertink, G.J. Vancso, Adv. Mater. 13 (2001) 1174–1178.
[2] M. Hehn, K. Ounadjela, J.P. Bucher, F. Rousseaux, D. Decanini, B. Bartenlian, C. Chappert, Science 272 (1996) 1782–1785.
[3] S. Kim, R. Asmatulu, H.L. Marcus, F. Papadimitrakopoulos, J. Colloid Interface Sci. 354 (15) (2011) 448–454.
[4] J.-K. Chen, J.-Y. Li, Sens. Actuators, B 150 (2010) 314–320.
[5] K.B. Lee, S.J. Park, C.A. Mirkin, J.C. Smith, M. Mrksich, Science 295 (2002) 1702–1705.
[6] J.K. Chen, C.H. Chan, F.C. Chang, Appl. Phys. Lett. 92 (2008) 053108.
[7] T.-Y. Chen, J.-K. Chen, Coloid Polym. Sci. 289 (2011) 433–445.
[8] J.-K. Chen, T.-Y. Chen, J. Colloid Interface Sci. 355 (15) (2011) 359–367.
[9] C.H. Chan, J.K. Chen, F.C. Chang, Sens. Actuators, B 13 (2008) 327–332.
[10] O. Lopez-Acevedo, K.A. Kacprzak, J. Akola, H. Hakkinen, Nat. Chem. 2 (2010) 329–334.
[11] M. Cao, M. Wang, N. Gu, J. Phys. Chem. C 113 (2009) 1217–1221.
[12] N. Erez, G. Gordon, M. Nest, G. Kurizki, Nature 452 (2008) 724–727.
[13] J.-K. Chen, J.-Y. Li, Appl. Phys. Lett. 97 (2010) 063701.
[14] A. Alivisatos, Science 271 (1996) 933–937.
[15] J.-K. Chen, F.-H. Ko, C.-H. Chan, C.-F. Huang, F.-C. Chang, Semicond. Sci. Technol. 21 (2006) 1213–1220.
[16] R.D. Piner, J. Zhu, F. Xu, S. Hong, C.A. Mirkin, Science 283 (1999) 661–663.
[17] T. Cuk, S.M. Troian, C.M. Hong, S. Wagner, Appl. Phys. Lett. 77 (2000) 2063.
[18] C.P.R. Dockendorf, T.Y. Choi, D. Poulikakos, A. Stemmer, Appl. Phys. Lett. 88 (2006) 131903-1.
[19] J.K. Chen, C.Y. Hsieh, C.F. Huang, P.M. Li, S.W. Kuo, F.C. Chang, Macromolecules 41 (2008) 8729–8736.
[20] M. Gessler, Y. Xia, Adv. Mater. 16 (2004) 1249–1269.
[21] D.-G. Choi, S. Kim, E. Lee, S.-M. Yang, J. Am. Chem. Soc. 127 (2005) 1636–1637.
[22] M. Albrecht, G. Hu, I.L. Guhr, T.C. Ulbrich, J. Boneberg, P. Leiderer, G. Schatz, Nat. Mater. 3 (2005) 203–204.
[23] A. Valsesia, P. Colpo, M.M. Silvan, T. Meziani, G. Ceccone, F. Rossi, Nano Lett. 4 (2004) 1047–1050.
[24] J.K. Chen, Z.Y. Chen, H.C. Lin, P.D. Hong, F.C.A.C.S. Chang, Appl. Mater. Interfaces 1 (2009) 1525–1532.
[25] M. Brust, M. Walker, D. Bethell, D.J. Schiffrin, R. Whyman, J. Chem. Soc., Chem. Commun. (1994) 801–802.
[26] J.-K. Chen, A.-L. Zhuang, J. Phys. Chem. C 114 (2010) 11801–11809.
[27] J.-K. Chen, C.-Y. Hsieh, C.-F. Huang, P.-M. Li, J. Colloid Interface Sci. 338 (2009) 428–434.
[28] G. Shafai, S.Y. Hong, M. Bertino, T.S. Rahman, J. Phys. Chem. C 113 (2009) 12072–12078.
[29] B. Adhikari, A. Banerjee, Chem. Mater. 22 (2010) 4364–4371.
[30] A. Longo, L.F. Liotta, G. Di Carlo, F. Giannici, A.M. Venezia, A. Martorana, Chem. Mater. 22 (2010) 3952–3960.
[31] I. Tunc, S. Suzer, M.A. Correa-Duarte, L.M. Liz-Marzán, J. Phys. Chem. B 109 (2005) 7597–7600.
[32] X. Zhuang, Q.F. Zhao, Y. Wan, J. Mater. Chem. 20 (2010) 4715–4724.
[33] S. Ko, Y. Choi, D.J. Hwang, C.P. Grigoropoulos, D. Poulikakos, Appl. Phys. Lett. 89 (2006) 141126–141128.
[34] A.P. Alivisatos, Science 271 (1996) 933–937.
[35] S. Ospelkaus, K.K. Ni, D. Wang, M.H.G. de Miranda, B. Neyenhuis, G. Quéméner, P.S. Julienne, J.L. Bohn, D.S. Jin, J. Ye, Science 327 (2010) 853–857.
[36] C.-W. Kuo, J.-Y. Shiu, P. Chen, G.A. Somorjai, J. Phys. Chem. B 107 (2003) 9950–9953.
[37] S. Kwon, X. Yan, A.M. Contreras, J.A. Liddle, G.A. Somorjai, J. Bokor, Nano Lett. 5 (2005) 2557–2562.
[38] R.T.R. Kumar, K.B. Mogensen, P. Bøggild, J. Phys. Chem. C 114 (2010) 2936–2940.
[39] L. Zhang, Z. Zhou, B. Cheng, J.M. DeSimone, E.T. Samulski, Langmuir 22 (2006) 8576–8580.